European Journal of Pharmaceutical Sciences 49 (2013) 400–410

Contents lists available at SciVerse ScienceDirect

European Journal of Pharmaceutical Sciences

journal homepage: www.elsevier.com/locate/ejps

Viscosity of high concentration protein formulations of monoclonal antibodies of the IgG1 and IgG4 subclass – Prediction of viscosity through protein–protein interaction measurements

Martin S. Neergaard [a,*], Devendra S. Kalonia [b], Henrik Parshad [c], Anders D. Nielsen [d], Eva H. Møller [a,1], Marco van de Weert [a]

[a] Section for Biologics, Department of Pharmacy, Faculty of Health and Medical Sciences, University of Copenhagen, Universitetsparken 2, Copenhagen, Denmark
[b] Department of Pharmaceutical Sciences, University of Connecticut, Storrs, CT 06269, United States
[c] Novo Nordisk, CMC Biopharm Analysis & Formulation, Hagedornsvej 1, Gentofte, Denmark
[d] Novo Nordisk, Protein Characterization, Biopharm, Novo Nordisk Park, Måløv, Denmark

ARTICLE INFO

Article history:
Received 15 November 2012
Received in revised form 16 April 2013
Accepted 17 April 2013
Available online 26 April 2013

Keywords:
Protein–protein interactions
Interaction parameter
Viscosity
Dynamic light scattering
High concentration formulation
Monoclonal antibody subclass

ABSTRACT

The purpose of this work was to explore the relation between protein–protein interactions (PPIs) and solution viscosity at high protein concentration using three monoclonal antibodies (mAbs), two of the IgG_4 subclass and one of the IgG_1 subclass. A range of methods was used to quantify the PPI either at low concentration (interaction parameter (k_D) obtained from dynamic light scattering, DLS) or at high concentration (solution storage modulus (G') from ultrasonic shear rheology). We also developed a novel method for the determination of PPI using the apparent radius of the protein at either low or high protein concentration determined using DLS. The PPI measurements were correlated with solution viscosity (measured by DLS using polystyrene nanospheres and ultrasonic shear rheology) as a function of pH (4–9) and ionic strength (10, 50 and 150 mM). Our measurements showed that the highest solution viscosity was observed under conditions with the most negative k_D, the highest apparent radius and the lowest net charge. An increase in ionic strength resulted in a change in the nature of the PPI at low pH from repulsive to attractive. In the neutral to alkaline pH region the mAbs behaved differently with respect to increase in ionic strength. Two mAbs (A and B) showed little or no effect of increasing ionic strength, whereas mAb-C showed a remarkable decrease in attractive PPI and viscosity.

Previous studies have mainly investigated mAbs of the IgG_1 and IgG_2 subclass. We show here, for the first time, that mAbs of the IgG_4 subclass behave similar as the other subclasses. By comparison of the three tested mAbs with mAbs investigated in other studies a clear linear trend emerges between the pH of strongest attractive PPI and highest solution viscosity. The determination of PPI using either k_D or apparent radius is thus a useful prediction tool in the determination of solution conditions that favors low solution viscosity at high protein concentration of therapeutically used mAb molecules. The novel methodology using apparent radius is a simple and rapid alternative to determine relative PPI directly under formulation conditions. The method can potentially serve as a high-throughput screening tool in formulation development.

© 2013 Elsevier B.V. All rights reserved.

Abbreviations: AA, amino acid; AUC, analytical ultracentrifugation; BSA, bovine serum albumin; cIEF, capillary isoelectric focusing; η^*, complex viscosity; *A*, crystal constant; DTS, Dispersion Technology Software; DLS, dynamic light scattering; FFR, fast field reversal; GdnHCl, guanidinium hydrochloride; TNP, hapten trinitrophenyl; r_H, hydrodynamic radius; k_D, interactions parameter; IV, intravenous; IS, ionic strength; pI, isoelectric point; M3, Mixed Mode Measurement; mAb(s), monoclonal antibody (ies); D_m, mutual diffusion coefficient; PALS, phase analysis light scattering; PDI, polydispersity index; PPI, protein-protein interactions; X_2, reactance; R_2, resistance; D_s, self-diffusion coefficient; SIC, self-interaction chromatography; SEC, size exclusion chromatography; SFR, slow field reversal; G'', solution loss modulus; G', solution storage modulus; SLS, static light scattering; SC, subcutaneous; TFF, tangential flow-filtration; TAG-72, tumor-associated glycoprotein 72; USR, Ultrasonic Shear Rheometry; UV, ultraviolet; η, viscosity.

* Corresponding author. address: Department of Pharmacy, Section of Biologics, Faculty of Health and Medical Sciences, University of Copenhagen, Universitetsparken 2, DK-2100 Copenhagen, Denmark. Tel.: +45 35 33 61 83; fax: +45 35 33 60 30.
E-mail address: martin.neergaard@sund.ku.dk (M.S. Neergaard).
[1] Present address: Novo Nordisk, CMC Diabetes Analysis and Formulation, Novo Nordisk Park, Måløv, Denmark.

0928-0987/$ - see front matter © 2013 Elsevier B.V. All rights reserved.
http://dx.doi.org/10.1016/j.ejps.2013.04.019

1. Introduction

During the last few decades therapeutic monoclonal antibodies (mAbs) have attracted significant attention from the pharmaceutical and biotech industries. From 1985 to 2011 mAbs have been among the fastest growing class of drugs in the pharmaceutical sector and novel mAbs are entering clinical studies at a record pace. Currently 31 therapeutic mAbs are approved worldwide (January 1st 2012) for treatment of a wide range of diseases including; transplant rejection, cancer, infections, allergies, cardiovascular disease and autoimmune-disorders like arthritis, psoriasis, multiple sclerosis and inflammatory bowel-diseases (Beck et al., 2010; Lowe et al., 2011; Nelson et al., 2010; Reichert, 2010, 2012; Warne, 2011). A large number of the mAbs currently approved are administered through intravenous injection (IV) which requires professional healthcare assistance or hospitalization. For products with frequent and chronic administration, the subcutaneous (SC) route of administration is more desirable. This would enable patient self-administration, increase the convenience and compliance of the treatment, and save the healthcare sector large expenses. However, mAb treatment requires relative large doses, often in the range of several mg/kg bodyweight. The volume restrictions (<1.5 mL) for SC injections, therefore, necessitates the development of high concentration formulations (Shire et al., 2004). With the development of high concentration formulations (>100 mg/kg), the formulation scientist faces a number of significant challenges including: impaired long term stability due to self-association and aggregation; processing, manufacturing and administration difficulties due high viscosities; and finally, a lack of readily available and applicable analytical methods for the direct characterization of these formulations (Kanai et al., 2008; Salinas et al., 2009; Shire et al., 2004; Yadav et al., 2010a).

The viscosity in low concentration conditions has been shown to depend on the net-charge of the protein molecule, with increasing viscosities as the molecule moves away from its pI (pH with net zero charge) (Yadav et al., 2011b). This behavior has been explained by the electroviscous effect due to the presence of an electrical double layer around the molecule, which influences the flow behavior of the molecule (Mcdonogh and Hunter, 1983). Recently, Yadav et al. (2011b) showed that high concentration formulations of bovine serum albumin (BSA) deviated from this trend showing increasing viscosity as solution pH approaches pI (Yadav et al., 2011b). Higher viscosity at pH values close to the pI has also been observed with high concentration mAbs (Saito et al., 2012; Saluja et al., 2006). Although they are structurally very similar, mAbs may differ significantly in various aspects including their aggregation behavior and rheological properties as exemplified by Kanai et al. (2008) and Yadav et al. (2010b, 2011c, 2012a,b).

The types of intermolecular interaction present in a protein solution do not deviate between low and high concentration, but the relative contribution is remarkably affected by the increase in protein concentration. The intermolecular distance is reduced as the concentration increases, which leads to an increasingly more important role of short range protein–protein interactions (PPIs). Ultimately short range interactions begin to dominate the flow behavior, and the viscosity is no longer explained by simple electroviscous effects (Saluja and Kalonia, 2008). The rheological behavior at high concentration protein formulations correlates well with the measured strength of protein–protein interactions (Saito et al., 2012; Saluja and Kalonia, 2005; Saluja et al., 2007b; Yadav et al., 2010a, 2012a, 2011c). A variety of different interactions are possible including; electrostatic, steric (excluded volume), hydrophobic and van der Waals interaction (including dipole interactions). In dilute solution conditions, where the intermolecular distance is large, charge-charge repulsive interactions generally contribute the most to the PPI (Chari et al., 2009; Saluja and Kalonia, 2008). The contribution of attractive forces (specific charge-charge interactions, hydrophobic interactions, van der Waals interactions) increases rapidly when the intermolecular separation distance is decreased.

PPI are traditionally quantified using non-ideality parameters such as the second virial coefficient (B_{22}) and the interaction parameter (k_D) in dilute solution conditions. More recently Kalonia and co-workers (Saluja et al., 2006, 2007b) justified the use of the storage modulus (G') measured by Ultrasonic Shear Rheometry (USR) as an indicator of PPI in high concentration solutions. Significant amounts of work have correlated (primarily) B_{22} to protein precipitation, solubility, crystallization, aggregation and liquid–liquid phase separation (Chi et al., 2003; Eberstein et al., 1994; George and Wilson, 1994; Ho et al., 2003; Muschol and Rosenberger, 1995; Ruppert et al., 2001; Valente et al., 2005). The most commonly used technique for determination of B_{22} values is static light scattering (SLS), but also analytical ultracentrifugation (AUC) (Liu et al., 2005), membrane osmometry (Salinas et al., 2009), size exclusion chromatography (SEC) (Bloustine et al., 2003), self-interaction chromatography (SIC) (Valente et al., 2005) and more recently dynamic light scattering (DLS) (Yadav et al., 2011a) are available for the determination of B_{22}. In contrast, k_D is only determined by DLS by plotting the mutual diffusion coefficient (D_m) against the protein concentration. Both B_{22} and k_D can be used to assess the nature of intermolecular interactions (Li et al., 2004). The value of B_{22} originates from the virial expansion of the ideal gas equation, its value reflects the magnitude of deviation from ideality and its sign shows the nature of this deviation. Positive B_{22} values correspond to repulsion between protein molecules, whereas a negative value shows that forces between molecules are attractive in nature (Muschol and Rosenberger, 1995; Neal et al., 1998). B_{22} measures the sum of interactions between protein molecules, including electrostatic, hard-sphere, van der Waals, and hydrophobic interactions. k_D is related to B_{22} through Eq. (7) (Section 2). B_{22} is a purely thermodynamic factor, whereas k_D also consists of a hydrodynamic contribution from the frictional drag (Harding and Johnson, 1985; Yadav et al., 2010a).

In this study we characterized the high concentration viscosity of three mAbs, one IgG_1 and two IgG_4s, at varying pH and ionic strength. To the best of our knowledge this is the first study to include antibodies of the IgG_4 subclass. A thorough rheological analysis of all therapeutically relevant mAb subclasses has now been conducted and we observe a clear linear trend in the comparison between the pH with strongest attractive PPI and the pH with highest solution viscosity when comparing the three molecules investigated in this study with results found in the literature. Furthermore, we present a novel method to determine PPI directly under formulation conditions using the apparent hydrodynamic radius at high protein concentrations measured by DLS.

2. Materials and methods

2.1. Model proteins

Three mAbs were used in this study, all manufactured by Novo Nordisk A/S. The antibodies B72.3 IgG_1 (mAb-A) and IgG_4 (mAb-B) recognize the antigen tumor-associated glycoprotein (TAG-72) and have been developed as a murine antibody of the IgG_1 subclass. The variable domains were cloned and transferred to human IgG_1 and IgG_4 constant domains. Antibody HzATNP (mAb-C) is a humanized IgG_4 antibody against the hapten trinitrophenyl (TNP). Both mAb-A and mAb-B have kappa (κ) light chains and the sequence identity in the light chain is therefore 100%. Sequence

PGR2026-00039
Biocon Ex.1033
Page 2 of 11

identity in the constant region of the heavy chain is approximately 95%. mAb-C, being an IgG_4, has a similar constant region as mAb-B, whereas the variable region shares only 45% sequence identity (including 9 inserts) with mAb-B.

All antibodies were purified using Protein A affinity chromatography follow by concentration and buffer-exchange (10 mM histidine buffer pH 6.5) using tangential flow-filtration (TFF).

2.2. Sample preparation

Low ionic strength buffers were prepared by dissolving 1.2 mM of each buffer species (citric acid, and monobasic phosphate) (Sigma–Aldrich – St. Louis, MO) in Milli-Q water. The pH (4–9) was adjusted with sodium hydroxide. The ionic strength was adjusted to 10 mM with sodium chloride (NaCl) (Merck – Darmstadt, Germany). Samples at the pH of interest were prepared using Millipore (Billerica, MA) Amicon Ultracentrifugation tubes with a molecular weight cut-off of 10kDa. After each buffer exchange and concentration to >150 mg/mL the pH was measured to confirm a successful buffer exchange. The pH of interest was generally reached within three to four cycles of buffer exchange. At the pH extremes (4.0 and 9.0) higher or lower pH buffers were used to reach the pH of interest. Higher ionic strength samples (50 and 150 mM) were prepared by adding a small amount of 5 M NaCl.

The protein concentration of the samples was determined using ultraviolet (UV) spectrometry using an extinction coefficient of 1.43 at 280 nm for 0.1% mAb-A/B solution and 1.48 for a 0.1% mAb-C solution.

The isoelectric point (pI) of each antibody was determined from capillary isoelectric focusing (cIEF) giving 8.6, 7.3 and 8.0 for mAb-A, -B, and -C, respectively.

2.3. Net charge and effective pI determinations

2.3.1. Zeta potential

Zeta potential (ζ) measurements were performed at 25 °C using a Malvern Zetasizer Nano ZS (Worchestershire, UK). All data analysis was performed using Dispersion Technology Software (DTS) V6.01. The zeta potential was measured at an antibody concentration of 5 mg/mL using a DTS1060 clear disposable folded capillary cell and a volume of 1 mL. Air bubbles, if present, were eliminated by gentle tapping of the cell. Three individual samples were averaged, all samples were filtered (0.22 μm) using Millex® – GV Syringe driven filter units (Millipore, Ireland). Per sample a maximum of 100 cycles were performed.

The zeta potential is calculated from the electrophoretic mobility (velocity of a particle in an electric field) and then applying the Henry equation:

$$U_E = \frac{2\varepsilon\zeta f(Ka)}{3\eta} \tag{1}$$

where U_E is the electrophoretic mobility under the applied voltage, ε is the dielectric constant of the medium (water 78.5), η is the viscosity of the dispersant (water at 25 °C, 0.8871 mPa s), ζ is the zeta potential in volts and $f(Ka)$ is the Henry's function. Two values are generally used as approximations for the $f(Ka)$ determination. Electrophoretic determinations of zeta potential in aqueous media and moderate electrolyte concentration uses a value of 1.5 for $f(Ka)$, and is referred to as the Smoluchowski approximation. For small particles in low dielectric constant media $f(Ka)$ becomes 1.0, this is referred to as the Hückel approximation. A $f(Ka)$ of 1 was used in the determination of ζ in this study.

Electrophoretic mobility was determined by laser Doppler velocimetry in combination with Mixed Mode Measurement (M3) and phase analysis light scattering (PALS). The M3 utilizes an alternating electric field in fast field reversal (FFR) and a slow field reversal (SFR) mode to avoid the interference of electro osmosis and improve the resolution of measurements, respectively.

The net charge on the protein was calculated using the electrophoretic mobility determined in the zeta potential measurements using the following equation:

$$Z = \frac{\mu k_B T}{D_S e} \cdot 3 \tag{2}$$

where μ is the electrophoretic mobility ($m^2/V\,s$), k_B is the Boltzmann constant (1.3807×10^{-23} J/K), T the temperature (298.15 K), D_s is the self-diffusion coefficient determined from linear plot using Eq. (6) and e is the elementary charge (1.6×10^{-19} C).

2.3.2. Theoretical determination of pI

The theoretical pI was calculated from the amino acid sequence using both SEDNTERP (http://www.bbri.org/RASMB/rasmb.html) and ExPASy (http://web.expasy.org/compute_pi/).

2.4. Protein–protein interactions and viscosity measurements

2.4.1. High-frequency ultrasonic rheology

The rheological properties of the antibodies were evaluated using an ultrasonic shear rheometer (USR). The measurements were conducted at 200 mg/mL protein concentration. Samples were measured in duplicate and error bars represent the difference between the two measurements conducted at each pH and IS. The theory and experimental procedure has been described in detail elsewhere (Saluja and Kalonia, 2004, 2005). Briefly, the instrument uses the piezoelectric properties of a quartz crystal vibration at a fundamental frequency of 10 MHz to characterize the liquid by recording the shifts in the series resistance (R_2) and reactance (X_2). The difference arising in the electrical properties of the crystal upon placing the liquid sample is used to calculate solution loss (G'') and storage (G') moduli and from this the complex viscosity (η^*) is calculated. For non-Newtonian viscoelastic fluids, the solution storage (G') and loss (G'') moduli are given by the following relationship (Saluja and Kalonia, 2005; Yadav et al., 2010a,b):

$$G'(\omega) = \frac{R_2^2 - X_2^2}{A^2 \rho Liq} \tag{3}$$

$$G''(\omega) = \frac{2R_2X_2}{A^2 \rho Liq} \tag{4}$$

The complex viscosity is calculated from the moduli determined above:

$$\eta^* = \frac{\sqrt{((G')^2 + (G'')^2)}}{\omega} = \frac{G^*}{\omega} \tag{5}$$

Each crystal was calibrated using glycerol–water mixtures of know density and viscosity to determine the crystal constant (A). After successful calibration, 35 μL of protein sample was placed on the center of the top electrode, ensuring the entire bottom electrode was covered, and the crystal was inserted in the crystal cover. The cover was surrounded by a water bath to maintain a constant temperature (25 °C) during the measurements and to avoid sample evaporation. 6 M guanidinium hydrochloride (GdnHCl) was used to clean the crystal between samples at similar solution conditions. Upon changing solution conditions, e.g. pH value, a more thorough cleaning was performed using chromic acid to removed adsorbed layers of protein.

PGR2026-00039
Biocon Ex.1033
Page 3 of 11

2.4.2. Dynamic light scattering

2.4.2.1. Determination of k_D. DLS studies were performed at 25 °C using a DynaPro Plate Reader equipped with an 830 nm laser source (Wyatt – Santa Barbara, CA). The software used was Dynamics V7, Version 7.1.0 (Wyatt). High concentration samples were diluted with the buffer of interest to obtain a concentration of 12 mg/mL and pH was measured to ensure stability. 5 M NaCl was spiked in during dilution to adjust solution ionic strength (IS) to 50 and 150 mM. 12 mg/mL samples were filtered through 0.22 μm filters (Millex® – GV – Millipore, Ireland) and diluted in filtered buffers (with desired pH and IS) to obtain lower concentration samples. 35 μL of sample was added to a 384 Well UV-Star® Clear Microplate (781801) (Greiner Bio-One GmbH, Germany). The plate was covered with a clear disposable tape, Topseal™ (Packard – Meriden, CT), to avoid evaporation during measurement. Prior to measurement all plates were centrifuged at 3000 rpm for 5 min using an Eppendorf Centrifuge 5810 R (Eppendorf AG, Hamburg). 10 acquisitions of each 5 s were measured for each sample with auto adjustment of attenuator and laser power. Three wells of each sample were averaged and all samples were measured in triplicate. Water was chosen as a standard solvent during all measurements.

The mutual diffusion coefficient, D_m (m^2/s) of the monomeric protein peak was plotted against the protein concentration (g/mL) to obtain the interaction parameter, k_D from the following equation:

$$D_m = D_s(1 + k_D C) \tag{6}$$

where D_s is the self-diffusion coefficient (the value of D_m at infinite dilution) and c is the protein concentration. D_s is obtained from the intercept of a plot of D_m versus c and k_D can be obtained from the slope.

k_D from Eq. (6) describes interparticle interactions and can be represented as:

$$k_D = 2MB_{22} - k_f - 2v \tag{7}$$

where M is the molecular weight, B_{22} is the second virial coefficient, v is the protein partial specific volume, and k_f is the first order concentration coefficient in the virial expansion of the frictional coefficient.

Assuming spherical shape of the molecules, D_s can be used to calculate the hydrodynamic radius (r_H) through the Stokes–Einstein equation:

$$D_s = \frac{k_B T}{6\pi\eta r_H} \tag{8}$$

where k_B is the Boltzmann constant, T is the solution temperature in Kelvin and η is the solvent viscosity.

2.4.2.2. Viscosity measurements using nanospheres. The viscosity of the high concentration antibody solutions was measured using the DLS method developed by He et al. (2010) (He et al., 2010). Plain polystyrene nanospheres with an average diameter of 206.5 nm ± 20.6 nm were obtained from Phosphorex (Fall River, MA). The accuracy of the method was tested using glycerol solutions in the concentration range 0–70%w/w. 25 μL of sample was added to a 384 Well UV-Star® Clear Microplate (781801) (Greiner Bio-One GmbH, Germany). The plate was covered with a clear disposable tape, Topseal™ (Packard – Meriden, CT), to avoid evaporation during measurement. Prior to measurement all plates were centrifuged at 3000 rpm for 5 min using an Eppendorf Centrifuge 5810 R (Eppendorf AG, Hamburg). 0.20 μL of beads (2.2×10^{13} - beads/mL) was added to 72 μL of protein solution to obtain a final bead concentration of 6×10^{10} beads/mL.

According to the Stokes–Einstein equation, for any given solution, diffusant, and temperature, the diffusion coefficient is dependent on the solution viscosity and radius of the beads. This enables calculation of the solution viscosity:

$$\eta_2 = \frac{\eta_1 R_1}{R_2} \tag{9}$$

where η_1 is the viscosity of water at 25 °C (0.893 cP), R_1 is the apparent radius of the beads from analysis of the autocorrelation function using viscosity η_1, and η_2 and R_2 represent the real solution viscosity and the known radius of the beads, respectively.

2.4.2.3. Size measurements. The size of the antibodies at varying pH and IS was determined at 150 mg/mL using the DynaPro Plate Reader (Wyatt – Santa Barbara, CA). 35 μL of sample was added to a 384 Well UV-Star® Clear Microplate (781801) (Greiner Bio-One GmbH, Germany). Three individual samples were analyzed. The monomeric protein peak was plotted against pH to give information about PPI. The size was compared with the hydrodynamic radius (calculated from D_s using the Stokes–Einstein equation). The relative size was calculated (apparent radius divided by hydrodynamic radius) to show the nature of the PPI. Values <1 correspond to repulsive PPI, whereas values >1 relate to attractive interactions.

3. Results

3.1. Isoelectric point and net-charge

Zetapotential measurements were used to determine the effective pI in solution. The results for the three mAb molecules are shown in Fig. 1. Table 1 compares the zeta potential results with those obtained by cIEF and the pI values predicted from the amino acid sequence using either SEDNTERP or ExPASy.

The results show that the effective pI determined from zeta potential measurements is generally approximately 1 pH unit lower compared to the values determined from cIEF. However, the individual ranking of the mAbs is the same irrespective of the method used. Moreover, the zeta-potential of mAb-C decreases faster as a function of pH compared to that of mAb-A and B.

MAb-C behaved differently around the pI compared to the other two antibodies. Whereas mAb-A and mAb-B were generally monodisperse with polydispersity index (PDI) <0.1, measurements for mAb-C between 6.5 < pH < 8.7 gave a much higher PDI. An additional peak at larger size was observed in the intensity distribution under these solution conditions (results not shown). Adjusting the pH of a monodisperse solution of mAb-C from pH 5.0 to pH 7.0 induced the formation of this fraction of self-associates. Doing the

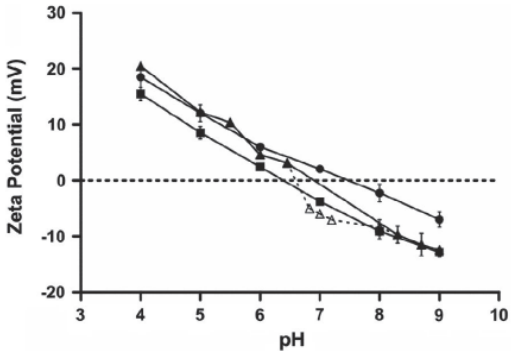


Fig. 1. Zeta potential of mAb solutions at varying pH, 10 mM ionic strength and 25 °C. Circles represent mAb-A, squares mAb-B and triangles mAb-C. Open triangles shows results that had unsatisfying polydispersity index (PDI) during measurement of the zeta potential, these were omitted in the determination of the effective pI.

Table 1
pI values predicted using theoretical calculation from amino acid sequence (ExPASy or SEDNTERP) and experimentally determined using cIEF (main peak) and zeta potential measurements.

mAb	AA (ExPASy)	AA (SEDNTERP)	cIEF (Main)	Effective pI
A	8.2	8.7	8.6	7.5
B	7.3	7.6	7.3	6.5
C	7.9	8.3	8.0	7.0

Table 2
Net charge on the three antibodies at varying pH as determined using Eq. (2).

pH	Net charge		
	mAb-A	mAb-B	mAb-C
4	15.8(±1.6)	13.1(±0.7)	17.2(±0.3)
5	10.2(±1.8)	7.5(±0.7)	10.1(±0.6)
6	5.1(±0.3)	2.1(±0.6)	3.8(±0.4)
7	1.8(±0.1)	3.2(±0.5)	4.9(±0.6)
8	1.9(±1.3)	7.7(±1.1)	7.1(±1.0)
9	5.8(±1.1)	10.9(±0.9)	10.2(±0.3)

opposite (adjusting a sample at pH 7.0 with PDI > 0.1 and an additional large size peak to lower pH) showed that these self-associates were reversible as the sample again appeared monodisperse (PDI < 0.1). These measurements with PDI > 0.1 are shown as open symbols in Fig. 1. From linear extrapolation, the effective pI is determined as the intercept with the abcissa axis. Results are summarized in Table 1.

The charge on each mAb at each pH value investigated is calculated using Eq. (2) and listed in Table 2.

3.2. Viscosity

3.2.1. Nanospheres

Low shear viscosity was measured using plain polystyrene nanospheres (Fig. 2A–C). We observed that mAb-A induced aggregation of the beads, especially at high ionic strength. There was a pronounced increase in viscosity at increasing IS, most pronounced at pH 8.0 (note the scale difference between mAb-A and the two other mAbs). The low IS viscosity of mAb-A was highest at pH 8.0 and gradually decreased as the pH was lowered.

mAb-B showed an increase in viscosity from pH 4.0 to 7.0 and a decrease from 7.0 to 9.0 at low IS conditions. Increasing the IS resulted in a more flat viscosity profile, with the exception of the viscosity at pH 4.0 where an increase in IS induced a sharp increase in viscosity.

mAb-C showed the highest viscosity at pH 7.0 followed by pH 8.0. A sharp decrease in viscosity is observed when the pH is increased to 9.0, while a more gradual decrease is observed when the pH is lowered to 4.0. The viscosity is remarkably decreased at all pH values by increasing the IS. The viscosity profile is almost flat at 150 mM IS, and located at a lower viscosity compared to mAb-B.

3.2.2. Complex viscosity – η^*(USR)

The solution complex viscosity (η^*) was calculated from the solution storage (G') and loss (G'') moduli according to Eq. (5). The results are shown in Fig. 2D–F. The $\eta^*$of mAb-A behaves very similar to the G' with maximum located at pH 7.0 of solution with IS of 10 mM and 50 mM, whereas the maximum was shifted to pH 6.0 at 150 mM IS. The η^* was increased with increasing IS at pH 4.0, 5.0 and 9.0, at pH 6.0 it remained unchanged, whereas the viscosity was decreased at pH 7.0 and 8.0.

mAb-B showed a maximum η^* at pH 6.0 and 7.0 (both had a η^* of 4.5 cP). pH 5.0 and 8.0 samples were almost unaffected by an increase in IS, pH 6.0 and 7.0 showed a decrease in η^* with increasing IS and at pH 9.0 the η^* was slightly increased. A steep increase was observed at pH 4.0. mAb-C showed a maximum η^* at pH 7.0, of which the magnitude is higher for mAb-C compared to mAb-A and B (4.8 cP for mAb-C versus 4.4 cP for mAb-A and 4.5 for mAb-B). The η^* is generally decreased with increasing IS; at 50 mM the viscosity was almost constant in the interval between pH 5.0 and 8.0. A further increase in IS gave a flat profile, with a slight increase at low pH. The increase at low pH is mainly due to increase in the solution G'' at these pH values (Fig. 2L).

3.3. Protein–protein interactions

3.3.1. Solution storage modulus – G′ (USR)

The solution storage modulus (G') is the elastic component of the complex viscosity. Solution G' was studied to give information about PPI in high concentration mAb solutions. Fig. 2G–I shows the solution G' at 200 mg/mL mAb solution at varying pH and IS. mAb-A shows a parabolic profile at low IS with a maximum G', meaning strongest interactions, at pH 7.0. Increasing the IS to 50 mM did not change this overall profile, but the G' at pH 4.0, 5.0 and 9.0 are slightly increased. At 150 mM the parabolic profile was maintained, but the maximum shifted to pH 6.0. The G' at pH 6.0 was unaffected by the increase in IS to 150 mM, whereas G' increased at pH 4.0 and 5.0 and decreased at pH 7.0, 8.0 and 9.0.

mAb-B had a rather flat profile from 5.0 to 7.0 at low IS, and G' decreased on both sides of this interval. Increasing IS decreased G' at all pH values with the exception of pH 4.0 where a dramatic increase was observed.

mAb-C shows a maximum G' at pH 8.0, but the profile from 6.0 to 8.0 is close to flat. A sharp decrease was observed at pH 9.0, a decrease is also seen at low pH values. The IS has a pronounced effect on the G' of mAb-C, with a pronounced decrease at all pH values except pH 4.0, where an increase is observed. The profile is flat at 150 mM IS and located at lower G' values compared to mAb-A and B.

3.3.2. Interaction parameter – k_D (DLS)

The k_D values were determined from linear fits of a plot of D_m as a function of concentration (data not shown) using Eq. (6). All obtained k_D values are plotted against solution pH in Fig. 2M–O.

mAb-A shows a positive k_D at pH 4.0 and 5.0 at low IS, indicating the presence of repulsive PPI. The repulsive forces are gradually decreased as the pH is increased and the k_D value at pH 6.0 is almost zero. When the pH is further increased PPI changes from being repulsive to attractive in nature. The most negative k_D (most attractive PPI) is obtained at pH 8.0 (16.3 mL/g). From pH 8.0 to 9.0 the k_D gradually become less negative again, meaning that the attractive forces are decreased. Increasing the IS of the solution from 10 to 50 and 150 mM changes the positive magnitude at pH 4.0; at 150 mM IS the k_D even changes to a negative value. At pH 5.0 an increase in IS from 10 to 50 mM is enough to change the nature of the PPI from repulsive to attractive. More attractive PPI are also the result of an increase in IS at pH 6.0, whereas minimal change is observed at pH 7.0–9.0.

mAb-B behaves similar to mAb-A, and shows a positive k_D at pH 4.0 and 10 mM IS; all other kD values are negative irrespective of pH and IS. The most attractive interactions are found between pH 6.0 and 7.0 (14.1 and 14.0 mL/g respectively). Increasing the IS changes the pH of strongest attactive PPI to pH 6.0 at 50 mM and pH 5.0 at 150 mM. Only minor changes in k_D are observed with increasing IS in the interval between pH 6.0 and 9.0.

mAb-C has a k_D vs. pH profile which is very similar to mAb-A at low IS, with a positive kD at pH 4.0 and 5.0, the magnitude of k_D decreasing to a minimum at pH 8.0 (20.2 mL/g), and a slightly less negative k_D at pH 9.0. However, the effect of increasing IS on k_D is remarkably different for mAb-C compared to mAb-A and

PGR2026-00039
Biocon Ex.1033
Page 5 of 11

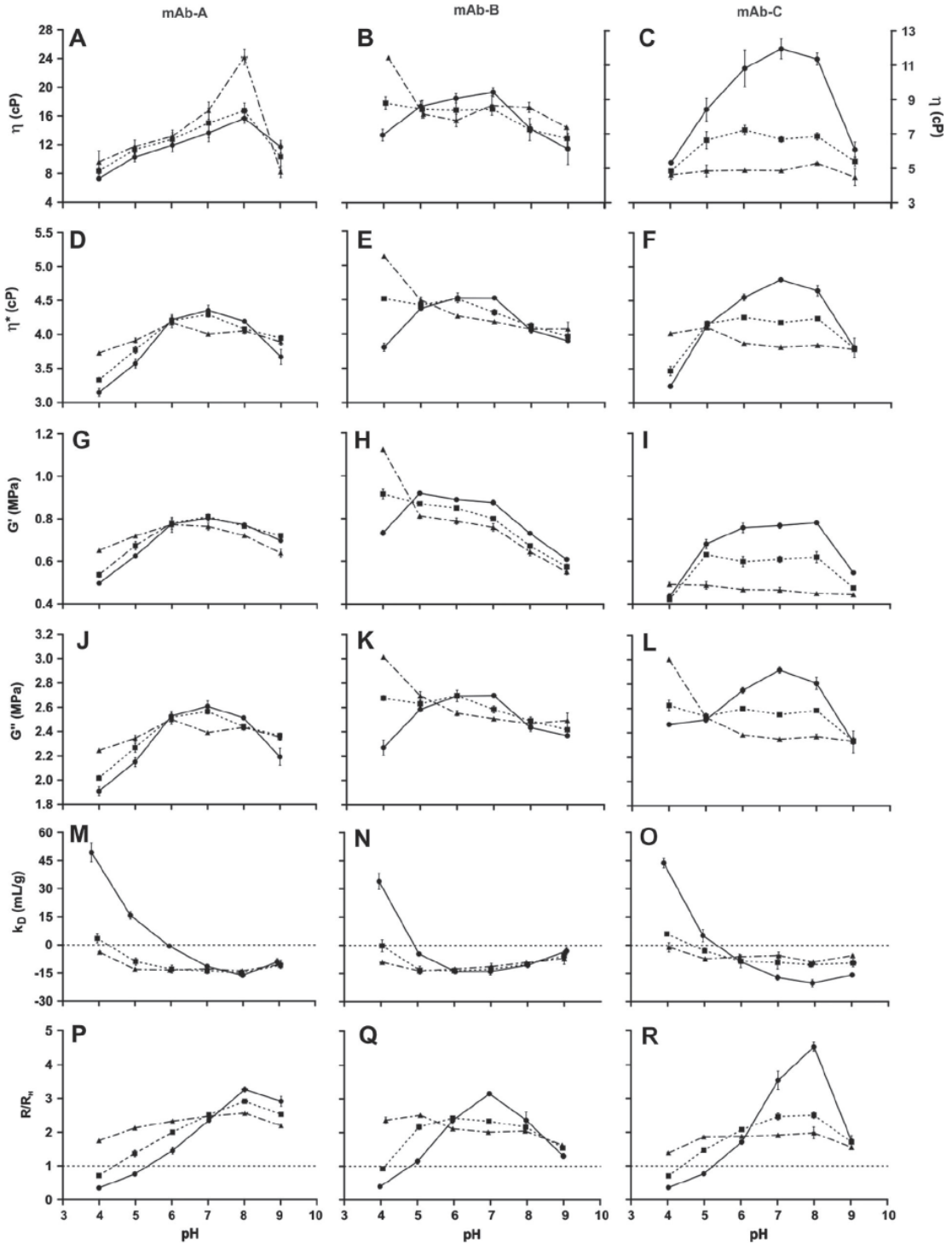


Fig. 2. Column 1: mAb-A, column 2: mAb-B. column 3: mAb-C. (A–C) shows the high concentration viscosity determined using DLS and polystyrene nanospheres. (D–F) shows the complex viscosity determined using USR. (G–I) shows the solution storage modulus (G') determined using USR. (J–L) shows the solution loss modulus (G'') determined using USR. (M–O) shows the interactions parameter (k_D) determined from linear fits to Eq. (6). (P–R) shows the apparent radius relative to the hydrodynamic radius (R_H). Circles and full line shows measurements at 10 mM ionic strength, squares and dotted line shows measurements at 50 mM ionic strength, and triangles and dashed-dotted line shows measurements at 150 mM ionic strength.

Table 3
Self-diffusion coefficient (D_s) determined from linear fits to Eq. (6) and hydrodynamic radius calculated using the Stokes–Einstein relation (Eq. (8)).

mAb	$D_s \times 10^{7}$ (cm^2/s)	r_H (nm)
A	4.80 ± 0.11	5.1 ± 0.11
B	4.89 ± 0.12	5.0 ± 0.13
C	4.89 ± 0.09	5.0 ± 0.09

mAb-B. The negative magnitude of kD is decreased dramatically when the IS is increased from 10 to 50 and 150 mM (17.2 to 9.2 to 5.5 mL/g at pH 7.0, 20.2 to 10.4 to 9.0 mL/g at pH 8.0 and 15.8 to 9.5 to 5.5 mL/g at pH 9.0). Little or no change is observe at pH 6.0, whereas the k_D is decreased at pH 4.0 and 5.0 upon increasing IS.

3.3.3. Size – relative radius

mAbs forms transient networks in high concentration solutions as a result of self-association of the molecules. The consequence of this self-association is that the molecule appears larger within the timeframe of the measurement (higher apparent radius as measured using DLS). From a simple size measurement, at any given concentration, information about PPI can be obtained by comparing the apparent radius with the real hydrodynamic radius of the molecule. This enables direct characterization of the nature of the PPI in the highly concentrated environment.

We determined the relative size of each antibody at 150 mg/mL using DLS. The obtained values are plotted as a function of pH and IS (Fig. 2P–R). The hydrodynamic radius was first determined from the self-diffusion coefficient (D_s) (average of D_s at pH 5.0–8.0 and 10, 50 and 150 mM IS) using the Stokes–Einstein relation (Eq. (8)) (Table 3).

mAb-A shows a maximum relative size at pH 8.0 irrespective of IS (Fig. 2P). The profile gradually becomes more flat as the IS is increased, but the overall profile is unchanged. Values below 1 represent repulsive interactions between molecules (size decreases with increasing concentration). Repulsion is observed at pH 4.0 at 10 and 50 mM IS and at pH 5.0 at 10 mM IS. All other combinations show attractive PPI. At pH 7.0 almost no change in relative size is observed with increasing IS. At pH 8.0 and 9.0 the effect is opposite, meaning that interactions are becoming less attractive with increasing IS.

mAb-B shows a maximum size at pH 7.0. Upon increasing IS the maximum shifts towards lower pH (pH 6.0 at 50 mM and pH 5.0 at 150 mM). There is a sharp increase in size at low pH (pH 4.0 and 5.0). The size is increased to a size larger than that of the higher pH values at high IS, which could indicate the presence of some strong attractive PPI. The effect of increasing pH at pH 6.0 and pH 8.0 is minimal, only a slight decrease is observed. At pH 9.0 a small increase is observed.

The size of mAb-C behaves somewhat different than mAb-A and B; the maximum is similar to that of mAb-A (pH 8.0), but the size is considerably larger than mAb-A. A sharp decrease in size is observed when increasing the pH from 8.0 to 9.0. The effect of increasing IS is strong at pH 7.0 and 8.0 and shows a large decrease in size, whereas almost no change in size is observed at pH 6.0 and 9.0. Large size increases were observed at low pH (4.0 and 5.0), where interactions change from being repulsive at low IS to attractive at high IS.

Fig. 3 compares the result of size measurements at 150 mg/mL and 12 mg/mL of mAb-B (Fig. 3A and B) and mAb-C (Fig. 3C and D). The general trend of changes in relative sizes as a function of pH and IS are similar at both concentrations, but with a slightly higher sensitivity at the high concentration.

4. Discussion

Until very recently the viscosity behavior of only two mAbs (one IgG_2 (Saluja et al., 2006) and one IgG_1 (mAb-1) (Liu et al., 2005; Yadav et al., 2010a)) have been comprehensively studied as a function of pH at high concentrations (>100 mg/mL). Yadav et al. (2011c) added an additional IgG_1 (mAb-2) and one mutant of mAb-1 and mAb-2 (Yadav et al., 2011c), later Yadav et al. (2012a) investigated two additional IgG_1s (mAb-2 and mAb-3) (Yadav et al., 2012a). Saito et al. (2012) investigated three mAbs, again all IgG_1, as a function of pH (Saito et al., 2012). This study investigated the viscosity behavior at high concentration and varying pH

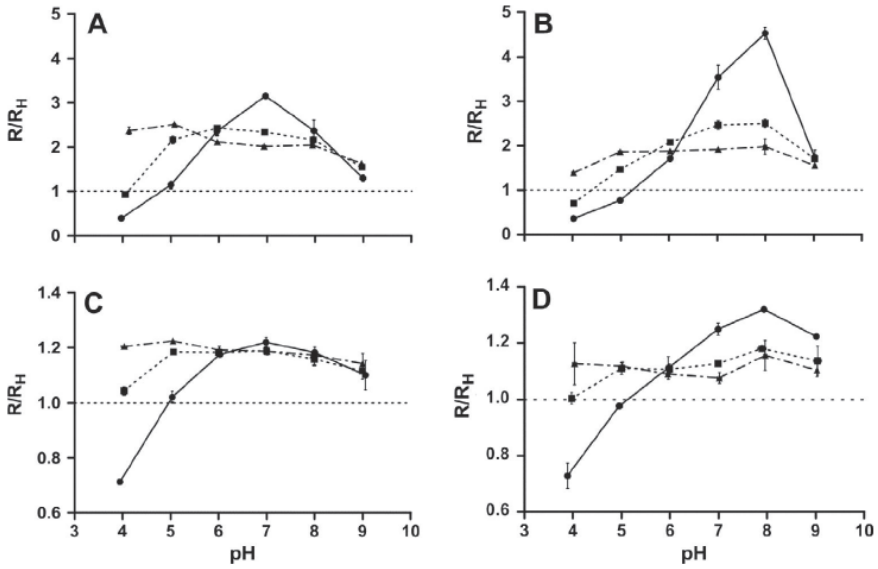


Fig. 3. Relative sizes plotted against solution pH. Left column shows mAb-B at 150 (A) and 12 mg/mL (C), right column shows mAb-C at 150 (B) and 12 mg/mL (D). Circles and solid line shows measurements at 10 mM ionic strength, squares and dotted line shows samples at 50 mM ionic strength and triangles and dashed-dotted lines shows samples at 150 mM ionic strength.

of one IgG_1 and two IgG_4 molecules. To the best of our knowledge this is the first study investigating IgG_4 mAbs at high concentration and varying pH.

4.1. pI, interactions, and viscosity

The viscosity measurements of the mAb solutions in this study were performed using two different methods. The first method, developed by He et al. (2010), employs DLS measurements on nanospheres, which allows a high sample throughput. The increase in relative size of these nanospheres can be backcalculated to solution viscosity using the Stokes–Einstein equation (He et al., 2010). The second method has been developed by Kalonia and co-workers and uses high-frequency ultrasonic rheology (Saluja et al., 2006; Saluja and Kalonia, 2004, 2005). The latter method also allows determination of the loss modulus (G'') and storage modulus (G') but is less amenable to high throughput measurements. One concern when using polystyrene nanospheres to measure solution viscosity is the possibility of spheres and protein interacting, forming protein-sphere complexes. He et al. (2010) mentioned this concern in their presentation of the method, but did not see any indication of interference from large protein aggregates or bead-protein interactions (He et al., 2010). In our study measurements on mAb-A did induce the formation of protein-sphere complexes, as evident from the remarkably high viscosity at pH 8.0 and high IS (Fig. 2A). This increase in viscosity was not observed using the USR method (Fig. 2D). It is out of the scope of this study to look further into this specific behavior of mAb-A, but the results emphasize the importance of being aware of this potential artifact for each specific protein.

The general trend in the viscosity measurements indicate that there is a pH, generally around neutral values, at which the viscosity is highest (Fig. 2A–F). The charge of a molecule is known to affect the viscosity of a solution through the electroviscous effect. The primary effect originates from the presence of an electric double layer and the water associated with this layer. This results in a slight increase in the hydrodynamic radius of the molecule and an increase in the resistance to flow. The secondary effect comes from the interactions of these double layers (Mcdonogh and Hunter, 1983; Salinas et al., 2009). Both of these effects will result in an increase in solution viscosity as the charge on the molecule increases (Saluja et al., 2007a). Tanford and Buzzell (1956) showed that the intrinsic viscosity of bovine serum albumin (BSA) was minimal at the pI of the molecule and increased at either side of pI due to an increase in the charge on the molecule (Tanford and Buzzell, 1956). Yadav et al. (2011b) showed similar results for BSA in dilute solution conditions. However, as the concentration increased to 250 mg/mL and the intermolecular distance decreased, the viscosity vs. concentration profile was reversed with maximum viscosity measured at the pI (Yadav et al., 2011b). Also in our studies and those of others the highest viscosity of high concentration mAb solutions is found close to the known pI of the mAb. This means that the viscosity behavior at high concentration is not due to net-charge induced primary or secondary electroviscous effects (Yadav et al., 2011b). Rather, this opposite effect of molecular charge on solution viscosity at high protein concentrations may be explained by the increased importance of short-range attractive interactions at high concentration. It has been shown that above 100 mg/ml and at low ionic strength the molecular surfaces of IgG_1 mAbs are in contact, allowing for these short-range attractive interactions to take place (Yadav et al., 2012a,b). A high net charge on the protein may cause repulsion between the mAbs and thus reduce the short-range interactions, resulting in lower viscosity when moving away from the pI.

This explanation is however incomplete, as it does not explain why the viscosity around the pI decreases significantly upon increasing the ionic strength of the formulation (Fig. 2A–F). This is discussed further below.

Fig. 4 shows that the effective pI determined from zeta potential measurements (Fig. 4A) is more predictive for the pH at which a high concentration solution viscosity is maximal than the pI determined from the amino acid sequence (Fig. 4B). The pI values determined from the zeta potential measurements are generally lower than those determined by capillary isoelectric focusing (cIEF) and the theoretically calculated value from the amino acid sequence (Table 1). This lower pI determined from electrophoretic mobility (zeta potential) measurements has previously been reported for several proteins (Chari et al., 2009; Lehermayr et al., 2011; Saluja et al., 2006; Yadav et al., 2010a). For the theoretically calculated values, this discrepancy has been explained by a failure of the algorithms to take into account the effect of the microenvironment of the charged amino acids, which will affect the pK_a of the amino acid. Chloride ion binding and concomittant lower pI has also been proposed as a possible explanation for selected mAbs (Saluja et al., 2006; Yadav et al., 2010a). In our experiments the pI determined from cIEF measurements most closely matched the values determined from the amino acid sequence. These values are determined as the pI of the main species of each mAb, and the cIEF results also showed that all of the mAbs investigated in this study had a significant amount of acidic species present (data not shown). Thus, another explanation for the lower effective pI is the presence of these acidic species. This suggests that zeta potential measurements may be a useful tool to predict the pH at which viscosity will be highest. However, the IgG_2 investigated by Saluja et al. (2006) and

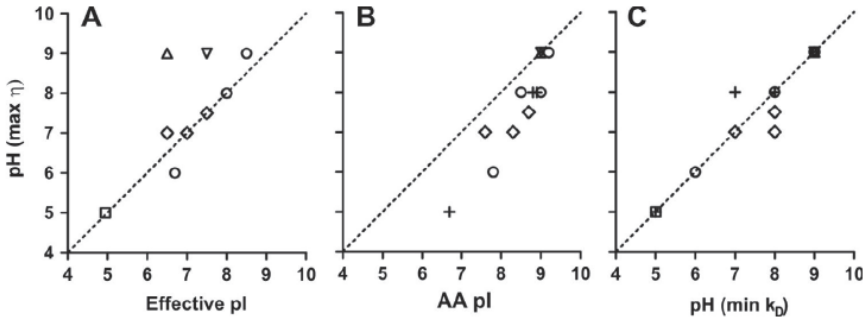


Fig. 4. Various correlations of pI (both effective from zeta potential (A) and theoretically calculated from amino acid sequence (B) and pH (min k_D) (C) with the pH of maximum viscosity. (circles) four IgG_1 from Yadav et al. (2012a,b) (viscosity determined using USR), (square) BSA from Yadav et al. (2012b) (viscosity determined using ViISCOlab 5000), (triangle) one IgG_2 from Saluja et al. (2006) (viscosity determined from USR), (reverse triangle) one IgG_2 from Chari et al. (2009) (viscosity determined from USR) (same mAb as Saluja et al. (2006), (diamonds) one IgG1 and two IgG4 from this study (viscosity determined using nanospheres and USR), and (crosses) three IgG1 from Saito et al. (2012) (viscosity determined using VROC). To guide the eye direct 1-to-1 linear relationships are added as dotted lines, these do not represent linear fits to the data.

PGR2026-00039
Biocon Ex.1033
Page 8 of 11

Chari et al. (2009) deviates from the general behavior of the other mAbs as seen in Fig. 4A (triangles). Here the pH of maximum viscosity deviates significantly from the determined effective pI. The latter was also much lower than expected, which was explained by chloride ion binding to the surface of the protein which affected the zeta potential measurements, but not PPI (k_D) or rheological properties (G' and η^*) (Chari et al., 2009; Saluja et al., 2006).

4.2. Prediction of high concentration viscosity from low and high concentration measurements

Although pI is generally a useful predictor of the pH of maximum viscosity (see above), it offers no insight into the magnitude and nature of the interactions and the variation of the viscosity with pH. To this purpose the determination of PPI is more informative. In general we observed a good qualitative correlation between the different methods of measuring PPI both those employed at low and high protein concentration. The strongest interactions for mAb-A are found at pH 8.0 (relative size and k_D) which correlates with the highest viscosity determined using the DLS and polystyrene nanospheres. The rheological method determines the strongest interactions at pH 7.0, which correlated with the maximum complex viscosity. The attractive interactions for mAb-B are strongest at a pH slightly lower than mAb-A; depending on the method this was at pH 7.0 (relative size), 6–7 (k_D) and 5 (G'). Relative size and k_D measurements correlate very well with the maximum viscosity, which was found at pH 7.0. All methods show maximum interactions at pH 8.0 for mAb-C, whereas the pH of maximum viscosity was found to be 7.0. A pronounced effect of IS on the PPI and viscosity of mAb-C was observed in all cases. mAb-C had a relative smaller size, a less negative k_D, a lower G' and a lower viscosity at high IS and neutral pH compared with mAb-A and B. In the low IS conditions this was opposite; here, mAb-C showed a higher relative size and a more negative k_D. This correlated with a higher viscosity of mAb-C solutions at low IS and neutral pH. mAb-B shows a strong interaction at low pH and high IS; the effect is most distinct when measuring in high concentration environment, signifying the increased contribution of short range PPI.

From Fig. 4C and a number of recent papers it is evident that the interaction parameter (k_D) is a useful parameter for prediction of high concentration viscosity behavior when investigating a single mAb molecule at varying pH (Saito et al., 2012; Yadav et al., 2012a). This applies to all therapeutically relevant mAb subclasses, including the IgG_1 and two IgG_4's from this study, as evident from Fig. 4C. The second virial coefficient (B_{22}) offers similar advantages (Saito et al., 2012), but the measurements are more cumbersome compared to the DLS method using the plate reader system. However, method development by Yadav et al. (2011a) has enabled the determination of B_{22} using a batch mode DLS instrument. We attempted to use similar measurements but found that our instrument performed a heterogeneous correction for laser power and attuation level depending on the position on the microtiter plate; this probably reflects the limitation of the photo diode detector used in this equipment and means that not all equipment is suitable for the method of Yadav et al. (2011a). An alternative approach is to calculate B_{22} based on a correlation with k_D as exemplified by Lehermayr et al. (2011).

It has previously been stated that the relation of k_D with high concentration viscosity is purely qualitative (Yadav et al., 2010b, 2012a). Yadav et al. (2010b) found that the negative magnitude of k_D did not correlate with the high concentration viscosity behavior (MAb-A vs. MAb-H in (Yadav et al., 2010b)). G' values determined at high protein concentration, on the other hand, did correlate with the behavior of the four MAbs investigated. The current study, however, does show that a more negative k_D (and a larger relative size) at the pH of greatest attractive interactions correlates with a higher viscosity at high protein concentration. Also the less negative k_D values for mAb-C at 150 mM ionic strength correlated with a lower viscosity (measured using nanospheres) at high concentration. mAb-C did, however, behave distinctly compared to the other mAbs investigated in the high frequency rheology measurements, as the G' values were not significantly larger compared to mAb-A and B. The viscosity increase was instead primarily mediated by the solution loss modulus (G'') leading to a less rigid solution structure.

Although the k_D and B_{22} measurements have predictive strength, they are not performed under true formulation conditions, as they require significant dilution of the high concentration mAb solution. We observed that the relative size of the mAb, as measured by DLS directly on the high concentration solution, was an equally strong predictor of the PPI (compare Fig. 2P–R with Fig. 2D–F). These measurements can also be performed at lower concentration, within the same range of the k_D determination, but require only a single concentration if the real hydrodynamic radius of the mAb is known. Note that the latter is effectively determined when doing the k_D analysis. The relative size measurements are significantly simpler than the other methods to determine PPI and can be used in a high throughput format using a plate reader at the actual concentration of interest. However, further studies are required to determine the robustness of this method.

4.3. Nature of PPI

The three antibodies used show a distinct viscosity behavior as a function of pH and IS, which is likely related to the effect of these parameters on the PPI. At neutral pH and dilute solution conditions mAb-A and mAb-B showed little effect of increasing IS. mAb-C on the other hand showed a dramatic drop in negative magnitude of k_D with increasing IS. The profile at 150 mM IS is almost flat, with the exception of pH 4.0. Using theoretical considerations Yadav et al. (2010b) showed that a k_D value with a less negative magnitude than 5.34 mL/g suggest that repulsion are the dominant interaction between molecules, whereas a value more negative than 5.34 mL/g indicate attraction between molecules (Yadav et al., 2010b). The k_D at high IS is approaching this value, showing that PPI are largely neutralized under these solution conditions. All methods show a pronounced viscosity-lowering effect of increasing salt concentration on mAb-C. The fact that the profile flattens at increasing IS shows that the attractive interactions are mainly of electrostatic origin (Yadav et al., 2012a). This suggests there are oppositely charged patches on this antibody that interact around the pI, resulting in the high viscosity.

Both mAb-A and B retain their pH-viscosity profile at high concentration upon increasing IS, which shows that the attractive interactions for these two antibodies are not electrostatic; for these mAbs the plausible interactions include various attractive dipole interactions, which are believed to dominate solution behavior at high concentration and high ionic strength where charge-charge interactions are screened (Chari et al., 2009; Liu et al., 2005; Saluja et al., 2007b; Yadav et al., 2010a).

mAb-B showed a dramatic increase in interactions at pH 4.0 and high IS. Here the increased attraction likely originates from interacting hydrophobic patches. Observations supporting this statement are a lower D_s value at pH 4 and high IS, which indicates that the molecule was slightly expanded, and a small deviation in the near-UV circular dichroism spectrum of this mAb at this pH value, indicating a slight perturbation of the native structure (results not shown). The strong interactions for mAb-B at pH 4.0 and 150 mM IS were not obvious in the measurements in dilute solution conditions (k_D did become negative, but the value was of a less magnitude than other solution conditions), confirming that the

PGR2026-00039
Biocon Ex.1033
Page 9 of 11

Table 4
Phase angles calculated from USR data of G' and G''.

pH	Ionic strength (mM)			Ionic strength (mM)			Ionic strength (mM)		
	10	50	150	10	50	150	10	50	150
	mAb-A			*mAb-B*			*mAb-C*		
4	75.4(±0.1)	75.1(±0.2)	73.8(±0.1)	72.1(±0.7)	71.1(±0.6)	69.6(±0.3)	77.7(±0.4)	78.8(±0.0)	78.8(±0.2)
5	73.8(±0.0)	73.4(±0.7)	72.9(±0.2)	70.4(±0.3)	71.4(±0.0)	73.2(±0.4)	74.8(±0.3)	76.0(±0.1)	79.1(±0.5)
6	72.9(±0.3)	72.8(±0.1)	72.8(±0.5)	71.8(±0.3)	72.5(±0.1)	72.8(±0.5)	74.6(±0.3)	77.0(±0.6)	78.9(±0.2)
7	72.9(±0.0)	72.5(±0.1)	72.3(±0.3)	72.0(±0.2)	72.8(±0.3)	73.2(±0.3)	75.2(±0.4)	76.6(±0.3)	78.8(±0.3)
8	72.8(±0.0)	72.6(±0.2)	73.5(±0.1)	73.3(±0.4)	74.9(±0.1)	75.4(±0.2)	74.4(±0.3)	76.5(±0.5)	79.3(±0.2)
9	72.3(±0.4)	73.0(±0.1)	74.8(±0.3)	75.6(±0.0)	76.6(±0.0)	77.5(±0.0)	76.8(±0.4)	78.5(±0.1)	79.2(±0.2)

interactions are short range attractive interactions, which are more dominant in the highly concentrated environment where charge–charge repulsions are mitigated by high concentration of salt.

The rheological behavior of mAb-C was different compared to mAb-A and B. An apparent higher viscosity was observed at low IS. This was not reflected in the magnitude of G' (Fig. 2I), which was at the same level as that of mAb-A and B. G'' values were, however, larger compared to those of mAb-A and B, and the main reason for the higher complex viscosity observed at the pI. High concentration mAb solutions are viscoelastic, meaning that the material shows both viscous and elastic properties (Janmey et al., 2007). Viscoelastic properties are characterized using G' and G'' referred to as the *storage* (*elastic*) *modulus* and *loss* (*viscous*) *modulus* respectively. The solution G' is a measure of the energy stored in the system and gives information about the rigidity of the interactions in solution. The increased rigidity in solutions with attractive interactions leads to an increase in solution G' compared to solutions in which repulsive interactions are dominating (Yadav et al., 2011c). The transient network in highly concentrated solutions of mAbs can be further characterized using the phase angle calculated as $\tan(\delta) = G''/G'$; these values are shown in Table 4.

Materials with phase angles above 45° ($G' < G''$), as in the case of the mAbs investigated in this study, show mostly liquid-like properties and most of the energy applied to the system is lost within one cycle of oscillation. What should be noted from Table 4 is that the phase angle at pH 4 and 150 mM IS for mAb-B is the lowest value observed, which could indicate that the interactions leading to the increase in G' cause the formation of an ordered network, which also leads to a significant increase in solution viscosity. We observed that mAb-B at pH 4 and 150 mM IS formed Thioflavin T positive aggregates upon incubation at 35 °C at 10 mg/mL, which further supports the formation of an highly ordered network under these solution conditions (results not shown). Formation of amyloid-like structures at acidic pH have previously been reported for an IgG_1 mAb (Brummitt et al., 2011). Another interesting observation is the higher phase angles of mAb-C, which shows that even though the viscosity of mAb-C was higher than mAb-A and B, the interactions leading to the increased viscosity are less rigid compared to the interactions in mAb-A and B solution. This indicates that the interactions present in mAb-C solutions are of a different origin compared with mAb-A and B, as also derived from the PPI measurements and the effect of IS.

5. Conclusion

The mAbs investigated in this study showed that it is possible to predict the pH of maximum viscosity at high protein concentration by quantifying PPI, for example through k_D or R/R_H. The general trend for a specific mAb is that a more negative k_D leads to a higher viscosity. Furthermore, it was shown that a lower net-charge (pH close to the pI) also correlated with higher solution viscosity. Interactions contributing to the high solution viscosity at high concentration are very dependent on the primary sequence and structure of the mAb. Moreover, the effective pI determined from zeta potential measurements was shown to be an important predictor of the pH with maximum viscosity. When a protein approaches its molecular pI the charge on the molecule is lowered, resulting in decreased charge-charge repulsion. This, in combination with a lower intermolecular separation distance, gives rise to short range attractive interactions that begin to dominate flow behavior of the solution. This appears to be a general trend when investigating proteins at high concentration, irrespective of the subclass of immunoglobulin G investigated.

Finally, the measurement of relative radius we presented as a tool to determine PPI at both low and high concentration may serve as a useful screening tool in high concentration formulation development. Further studies are required to assure its robustness towards varying formulation conditions and its predictive nature of the PPI for other mAbs than those tested here.

Acknowledgements

We greatly acknowledge Novo Nordisk and the Drug Research Academy at the University of Copenhagen for funding the project. Furthermore Novo Nordisk is acknowledged for the manufacturing of the antibodies used in this study. The Danish Ministry of Science, Technology and Innovation partly funded the Malvern Zetasizer Nano ZS MSN is grateful for the travel grants from Oticon fonden, Knud Højgaards Fond, Apoteker Sigurd Lunds og Hustru Ellen F. Højriis' mindelegat and Det Pharmaceutiske Understøttelses selskab in connection with his stay at the University of Connecticut.

References

Beck, A., Wurch, T., Bailly, C., Corvaia, N., 2010. Strategies and challenges for the next generation of therapeutic antibodies. Nat. Rev. Immunol. 10, 345–352.
Bloustine, J., Berejnov, V., Fraden, S., 2003. Measurements of protein–protein interactions by size exclusion chromatography. Biophys. J. 85, 2619–2623.
Brummitt, R.K., Nesta, D.P., Chang, L., Chase, S.F., Laue, T.M., Roberts, C.J., 2011. Nonnative aggregation of an IgG1 antibody in acidic conditions: Part 1. Unfolding, colloidal interactions, and formation of high-molecular-weight aggregates. J. Pharm. Sci. 100, 2087–2103.
Chari, R., Jerath, K., Badkar, A., Kalonia, D., 2009. Long- and short-range electrostatic interactions affect the rheology of highly concentrated antibody solutions. Pharm. Res. 26, 2607–2618.
Chi, E.Y., Krishnan, S., Kendrick, B.S., Chang, B.S., Carpenter, J.F., Randolph, T.W., 2003. Roles of conformational stability and colloidal stability in the aggregation of recombinant human granulocyte colony-stimulating factor. Protein Sci. 12, 903–913.
Eberstein, W., Georgalis, Y., Saenger, W., 1994. Molecular interactions in crystallizing lysozyme solutions studied by photon correlation spectroscopy. J. Cryst. Growth 143, 71–78.
George, A., Wilson, W.W., 1994. Predicting protein crystallization from a dilute solution property. Acta Crystallogr. D Biol. Crystallogr. 50, 361–365.
Harding, S.E., Johnson, P., 1985. The concentration-dependence of macromolecular parameters. Biochem. J. 231, 543–547.
He, F., Becker, G.W., Litowski, J.R., Narhi, L.O., Brems, D.N., Razinkov, V.I., 2010. High-throughput dynamic light scattering method for measuring viscosity of concentrated protein solutions. Anal. Biochem. 399, 141–143.
Ho, J.G., Middelberg, A.P., Ramage, P., Kocher, H.P., 2003. The likelihood of aggregation during protein renaturation can be assessed using the second virial coefficient. Protein Sci. 12, 708–716.

PGR2026-00039
Biocon Ex.1033
Page 10 of 11

Janmey, P.A., Georges, P.C., Hvidt, S., 2007. Basic rheology for biologists. Methods Cell Biol. 83, 3–27.
Kanai, S., Liu, J., Patapoff, T.W., Shire, S.J., 2008. Reversible self-association of a concentrated monoclonal antibody solution mediated by Fab–Fab interaction that impacts solution viscosity. J. Pharm. Sci. 97, 4219–4227.
Lehermayr, C., Mahler, H.C., Mader, K., Fischer, S., 2011. Assessment of net charge and protein-protein interactions of different monoclonal antibodies. J. Pharm. Sci. 100, 2551–2562.
Li, S., Xing, D., Li, J., 2004. Dynamic light scattering application to study protein interactions in electrolyte solutions. J. Biol. Phys., 313–324.
Liu, J., Nguyen, M.D., Andya, J.D., Shire, S.J., 2005. Reversible self-association increases the viscosity of a concentrated monoclonal antibody in aqueous solution. J. Pharm. Sci. 94, 1928–1940.
Lowe, D., Dudgeon, K., Rouet, R., Schofield, P., Jermutus, L., Christ, D., 2011. Aggregation, stability, and formulation of human antibody therapeutics. Adv. Protein Chem. Struct. Biol. 84, 41–61.
Mcdonogh, R.W., Hunter, R.J., 1983. The primary electroviscous effect. J. Rheol. 27, 189–199.
Muschol, M., Rosenberger, F., 1995. Interactions in undersaturated and supersaturated lysozyme solutions: static and dynamic light scattering results. J. Chem. Phys. 103, 10424–10432.
Neal, B.L., Asthagiri, D., Lenhoff, A.M., 1998. Molecular origins of osmotic second virial coefficients of proteins. Biophys. J. 75, 2469–2477.
Nelson, A.L., Dhimolea, E., Reichert, J.M., 2010. Development trends for human monoclonal antibody therapeutics. Nat. Rev. Drug Discov. 9, 767–774.
Reichert, J.M., 2010. Antibodies to watch in 2010. MAbs. 2, 84–100.
Reichert, J. M., 2012. About mAbs, (accessed 12.11.12) <http://www.landesbioscience .com/journals/Abs/about/>.
Ruppert, S., Sandler, S.I., Lenhoff, A.M., 2001. Correlation between the osmotic second virial coefficient and the solubility of proteins. Biotechnol. Prog. 17, 182–187.
Saito, S., Hasegawa, J., Kobayashi, N., Kishi, N., Uchiyama, S., Fukui, K., 2012. Behavior of monoclonal antibodies: relation between the second virial coefficient (B22) at low concentrations and aggregation propensity and viscosity at high concentrations. Pharm. Res. 29, 397–410.
Salinas, B.A., Sathish, H.A., Bishop, S.M., Harn, N., Carpenter, J.F., Randolph, T.W., 2009. Understanding and modulating opalescence and viscosity in a monoclonal antibody formulation. J. Pharm. Sci. 99, 82–93.
Saluja, A., Kalonia, D.S., 2004. Measurement of fluid viscosity at microliter volumes using quartz impedance analysis. AAPS. PharmSciTech. 5, e47.
Saluja, A., Kalonia, D.S., 2005. Application of ultrasonic shear rheometer to characterize rheological properties of high protein concentration solutions at microliter volume. J. Pharm. Sci. 94, 1161–1168.
Saluja, A., Kalonia, D.S., 2008. Nature and consequences of protein–protein interactions in high protein concentration solutions. Int. J. Pharm. 358, 1–15.
Saluja, A., Badkar, A.V., Zeng, D.L., Nema, S., Kalonia, D.S., 2006. Application of high-frequency rheology measurements for analyzing protein–protein interactions in high protein concentration solutions using a model monoclonal antibody (IgG2). J. Pharm. Sci. 95, 1967–1983.
Saluja, A., Badkar, A.V., Zeng, D.L., Kalonia, D.S., 2007a. Ultrasonic rheology of a monoclonal antibody (IgG2) solution: implications for physical stability of proteins in high concentration formulations. J. Pharm. Sci. 96, 3181–3195.
Saluja, A., Badkar, A.V., Zeng, D.L., Nema, S., Kalonia, D.S., 2007b. Ultrasonic storage modulus as a novel parameter for analyzing protein–protein interactions in high protein concentration solutions: correlation with static and dynamic light scattering measurements. Biophys. J. 92, 234–244.
Shire, S.J., Shahrokh, Z., Liu, J., 2004. Challenges in the development of high protein concentration formulations. J. Pharm. Sci. 93, 1390–1402.
Tanford, C., Buzzell, J.G., 1956. The viscosity of aqueous solutions of Bovine Serum Albumin between pH 4.3 and 10.5. J. Phys. Chem. 60, 225–231.
Valente, J.J., Payne, R.W., Manning, M.C., Wilson, W.W., Henry, C.S., 2005. Colloidal behavior of proteins: effects of the second virial coefficient on solubility, crystallization and aggregation of proteins in aqueous solution. Curr. Pharm. Biotechnol. 6, 427–436.
Warne, N.W., 2011. Development of high concentration protein biopharmaceuticals: the use of platform approaches in formulation development. Eur. J. Pharm. Biopharm. 78, 208–212.
Yadav, S., Liu, J., Shire, S.J., Kalonia, D.S., 2010a. Specific interactions in high concentration antibody solutions resulting in high viscosity. J. Pharm. Sci. 99, 1152–1168.
Yadav, S., Shire, S.J., Kalonia, D.S., 2010b. Factors affecting the viscosity in high concentration solutions of different monoclonal antibodies. J. Pharm. Sci. 99, 4812–4829.
Yadav, S., Scherer, T.M., Shire, S.J., Kalonia, D.S., 2011a. Use of dynamic light scattering to determine second virial coefficient in a semidilute concentration regime. Anal. Biochem. 411, 292–296.
Yadav, S., Shire, S., Kalonia, D., 2011b. Viscosity analysis of high concentration Bovine Serum Albumin aqueous solutions. Pharm. Res. 28, 1973–1983.
Yadav, S., Sreedhara, A., Kanai, S., Liu, J., Lien, S., Lowman, H., Kalonia, D., Shire, S., 2011c. Establishing a link between amino acid sequences and self-associating and viscoelastic behavior of two closely related monoclonal antibodies. Pharm. Res. 28, 1750–1764.
Yadav, S., Shire, S.J., Kalonia, D.S., 2012a. Viscosity behavior of high-concentration monoclonal antibody solutions: correlation with interaction parameter and electroviscous effects. J. Pharm. Sci. 101, 998–1011.
Yadav, S., Laue, T.M., Kalonia, D.S., Shire, S.J., 2012b. The influence of charge distribution on self-association and viscosity behavior of monoclonal antibody solutions. Mol. Pharm. 9, 791–802.

PGR2026-00039
Biocon Ex.1033
Page 11 of 11